УДК 550.348.098.4 DOI: https://doi.org/10.24028/gj.v47i6.333550

Focal mechanism of the November 9, 2023, M_w 4.1 earthquake in northern Thailand determined by full-waveform inversion

K. Saetang[1], W. Srisawat[2], 2025

[1]Nakhon Si Thammarat Rajabhat University, Nakhon Si Thammarat, Thailand
[2]Watthapho Municipal School, Nakhon Si Thammarat, Thailand
Received 25 June 2025

A M_w 4.1 earthquake occurred in northern Thailand (19.498°N, 98.518°E) on 09 November 2023 (centroid time: 07:30:19.86 UTC), within the seismically active Shan-Thai terrane. Source parameter determination employed full-waveform inversion utilizing three-component seismic data from ten regional stations at distances of 73—108 km, operated by the Thai Meteorological Department's seismic monitoring network, the Department of Mineral Resources network of Thailand, and the Myanmar National Seismic Network. The inversion methodology utilized the ISOLA software package, implementing iterative deconvolution based on the six-element moment tensor framework, and incorporated a minimal 1D velocity model with station corrections specifically calibrated for northern Thailand. Data preprocessing included instrumental response removal, baseline corrections, and band-pass filtering. Green's functions were computed using the frequency-wave number integration technique within a 0.03—0.10 Hz frequency band. Moment tensor inversion yielded a predominantly strike-slip mechanism with two nodal planes: plane 1 (strike=1°, dip=59°, rake=–148°) and plane 2 (strike=253°, dip=63°, rake=–35°) with 75 % double-couple and –1.2 % CLVD components. Grid search analysis systematically explored source depths from 0—35 km and determined an optimal centroid depth of 2.5 km, with maximum correlation coefficients exceeding 0.4 within the 2—4 km depth range. Waveform analysis demonstrates variance reduction values ranging from 0.40 to 0.80 at near-regional stations (Δ<250 km), indicating robust source parameter determination. The focal mechanism and seismicity distribution indicate strain release along an NE-SW trending structure, located 17 km west of the N-S trending Wiang Haeng fault system.

Key words: focal mechanism, full-waveform inversion, minimal 1D velocity model, northern Thailand, seismotectonics.

Introduction. The Sunda plate of Southeast Asia exhibits a complex pattern of present-day stress fields, with Thailand, Vietnam, and the Malay Basin characterized by predominantly north-south maximum horizontal stress orientation, consistent with the radiating stress patterns arising from the eastern Himalayan syntaxis [Tingay et al., 2010]. Additionally, Morley et al. [2011] provide a complementary framework for interpreting these stress regimes, illustrating how inherited basement fabrics, multi-episodic fault reactivation, and basin inversions during the Cenozoic evolution of Thailand exert a critical influence on modern deformation patterns. Consequently, focal mechanisms with oblique-slip components in northern Thailand and adjacent regions can be understood in the context of both the contemporary north-south compressional stress [Tingay et

Citation: Saetang, K., & Srisawat, W. (2025). Focal mechanism of the November 9, 2023, M_w 4.1 earthquake in northern Thailand determined by full-waveform inversion. *Geofizychnyi Zhurnal*, *47*(6), 15—25. https://doi.org/10.24028/gj.v47i6.333550.

al., 2010] and the reactivation of older fault systems [Morley et al., 2011].

The geodetic analysis of Simons et al. [2007] demonstrated systematic variation in Sundaland-Eurasia relative motion, characterized by differential eastward velocities ranging from 6±1 mm/yr in the south to 10±1 mm/yr in the north (ITRF2000 reference frame). While the Sunderland Block demonstrates predominantly coherent behavior, quantifiable elastic strain accumulation is evident along its convergent boundaries. The spatial distribution of GPS-derived velocity fields correlates with two key tectonic elements: the north-south-oriented maximum horizontal stress (σH_{max}) regime established through stress field analysis [Tingay et al., 2010] and the preferential reactivation of pre-existing structural discontinuities [Morley et al., 2011].

Following the 2004 M_w 9.1 Sumatra-Andaman earthquake, seismic monitoring capabilities in Thailand have been significantly enhanced through the expansion of two primary seismic networks. The Thai Meteorological Department has established a network of 71 seismic stations, and the Department of Mineral Resources has deployed 25 stations across the country [Seismic Monitoring Stations in Thailand, 2024; Seismic Station Network, 2024]. These independently operated networks have contributed to improved earthquake detection and location determination capabilities throughout Thailand.

Historical seismicity data (2009-Nov 2024) obtained from Thai Meteorological Department [Earthquake Catalog for Thailand and Adjacent Regions, 2024] comprise 11,609 events across mainland Southeast Asia, with magnitudes ranging approximately M 1.0—7.0 (Fig. 1). The study area occupies a complex transition zone between the Western Burma Terrane (WBT) and Sibumasu-Shan-Thai Terrane (STT), characterized by NE-SW trending fault systems in the east (Mae Yom and Uttaradit fault zones) and a combination of N-S (Mae Hong Son) and NW-SE trending structures (Mae Ping fault zone).

The seismotectonic framework of northern Thailand has been progressively refined through multiple seismological analyses. Receiver function studies have demonstrated that crustal thickness systematically increases from approximately 31 km beneath the Shan-Thai terrane in the west to 38 km beneath the Khorat Plateau of the Indochina terrane in the east, with major crustal discontinuities controlled by terrane boundaries [Noisagool et al., 2014]. Three-dimensional *P*- and *S*-wave velocity models derived from local earthquake tomography revealed spatially heterogeneous crustal structure, with low-velocity anomalies correlating with geothermal provinces and basin locations [Saetang et al., 2018]. The development of a minimum 1D velocity model with station corrections has enabled more precise earthquake location, with *P*-wave velocities ranging from 5.73 to 7.04 km/s and *S*-wave velocities from 3.35 to 4.00 km/s [Saetang, Duerrast, 2023]. Focal mechanism analysis of three selected aftershocks (M_w 4.1—5.0) from the 2014 M_w 6.3 Chiang Rai earthquake sequence revealed predominantly strike-slip faulting with a reverse component (strike=234÷244°, dip=67÷86°) along the Phayao Fault Zone [Saetang, 2017]. Seismic anisotropy investigations using shear wave splitting measurements from XKS phases revealed a complex two-layer anisotropic structure beneath northern Thailand, with fast polarization directions of –70° and 20° in the upper layer and –60° to 50° in the lower layer [Saetang, 2022].

This investigation presents a detailed focal mechanism analysis using full-waveform inversion techniques for a M_w 4.1 earthquake (19.498°N, 98.518°E) that occurred west of the mapped surface traces of the N-S trending Wiang Haeng fault zone on 9 November 2023. This event was selected from the regional seismicity catalog based on: (1) magnitude sufficiently large (M_w 4.1) to generate high-quality regional waveforms suitable for full-waveform inversion; (2) excellent azimuthal coverage from three networks; (3) epicentral location in a region lacking previous focal mechanism constraints; and (4) high signal-to-noise ratio recordings across multiple stations. The application of full-waveform inversion incorporates complete wavefield

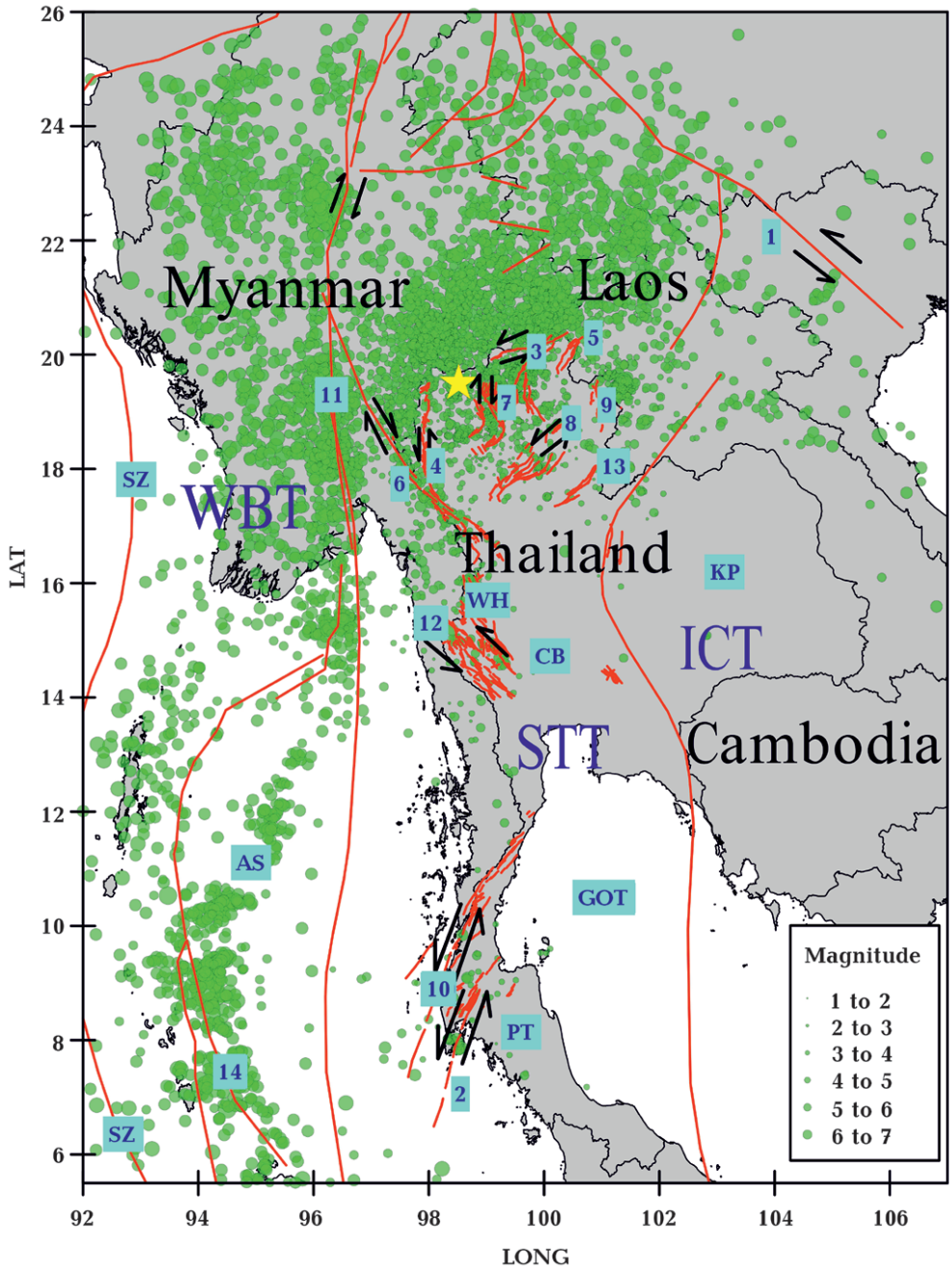

1 – Ailao Shan-Red River Shear zone
2 – Khlong Marui Fault zone
3 – Mae Chan Fault zone
4 – Mae Hong Son Fault zone
5 – Mae Ing Fault zone
6 – Mae Ping Fault zone
7 – Mae Tha Fault zone
8 – Mae Yom Fault zone
9 – Pua Fault zone
10 – Ranong Fault zone
11 – Sagaing Fault zone
12 – Three Pagodas Fault zone
13 – Uttaradit Fault zone
14 – Great Sumatran Fault zone
AS – Andaman Sea
CB – Central Basin
GOT – Gulf of Thailand
KP – Khorat Plateau
PT – Peninsular Thailand
SZ – Subduction Zone
WH – Western Highlands

Fig. 1. Seismotectonic framework of mainland Southeast Asia showing major fault systems and instrumentally recorded seismicity (2009-Nov 2024, M 1—7; green circles) from the Thai Meteorological Department network. The yellow star denotes the November 9, 2023, M_w 4.1 earthquake epicenter in the study area. Active faults (red lines [Geological Map of Thailand, 2007; Morley et al., 2011]) are numbered 1—14. Major tectonic terranes (WBT: Western Burma; ICT: Indochina; STT: Sibumasu/Shan-Thai) and geographic features (AS, CB, GOT, KP, PT, SZ, WH) are labeled.

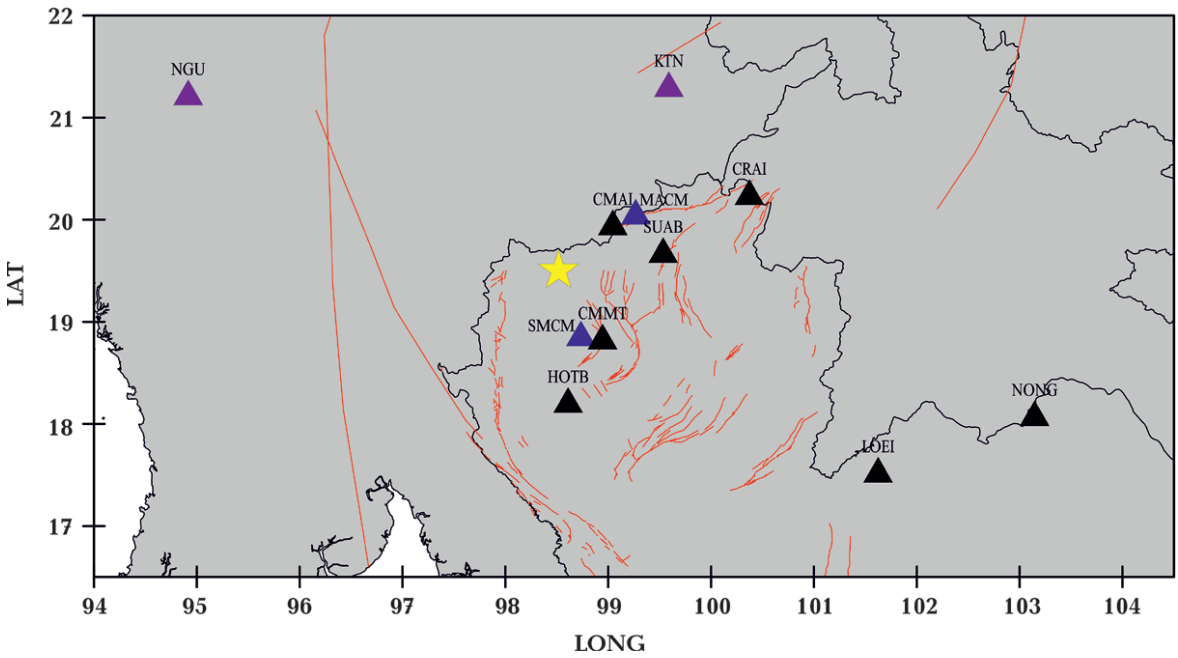

Fig. 2. Regional seismic station distribution used in this study. Black triangles denote stations of the Thai Meteorological Department (TM) network, blue triangles represent stations from the Department of Mineral Resources (TH) network, and purple triangles indicate stations from the Myanmar National Seismic Network (MM). The yellow star indicates the epicenter of the November 9, 2023, M_w 4.1 earthquake. Active faults are shown as red lines.

information, providing robust source parameter determination when combined with a recently developed minimal 1D velocity model specific to northern Thailand. The epicentral location relative to known structural features provides new constraints on active deformation patterns within this complex tectonic domain. Our objectives include precise determination of source parameters through systematic grid-search procedures, evaluation of solution stability through synthetic tests, and interpretation of results within the regional seismotectonic framework. This study represents the first comprehensive analysis of earthquake source parameters using full-waveform inversion in the study area.

Data and Methods. The seismic data analyzed in this study were obtained from three regional seismic networks deployed across northern Thailand and adjacent regions (Fig. 2): the Thai Meteorological Department's seismic monitoring network (TM), the Department of Mineral Resources network of Thailand (TH), and the Myanmar National Seismic Network (MM). The integrated network configuration provides comprehensive azimuthal coverage around the epicentral region. Data from public stations were accessed via the Incorporated Research Institutions for Seismology database, while restricted data from TM and TH networks were acquired through direct collaboration with the respective Thai government agencies. This multi-network approach provides comprehensive coverage of the study area and strengthens the robustness of our analysis.

Initial earthquake locations were determined through manual picking of *P*- and *S*-wave arrival times from ten high-quality recordings at regional distances of 73—108 km (Table 1). The location solution yields an RMS travel-time residual of 0.19 s, indicating good agreement between observations and theoretical arrival times computed using the minimum 1D velocity model with station corrections developed by Saetang and Duerrast [2023]. We employed the HYPOCENTER algorithm [Lienert et al., 1986; Lienert, Havskov, 1995], implemented within the Seisan software package [Havskov, Ottemöller, 1999], which utilizes a centered, scaled, and adaptively damped least-squares methodology for

hypocentral determination. In the subsequent waveform inversion analysis, while maintaining the epicentral coordinates (latitude and longitude) derived from HYPOCENTER, we performed a systematic grid search for source depths, exploring from 0.5 to 35 km at 0.5 km intervals.

Focal mechanism analysis was conducted using the ISOLA software package [Sokos, Zahradník, 2008], which implements an iterative deconvolution methodology based on the six-element moment tensor framework of Kikuchi and Kanamori [1991] and inverse problem formulation of Zahradník and Plešinger [2005]. Our analysis treated each earthquake as a centroid source, utilizing full waveform inversion techniques to determine the complete moment tensor solution. The inversion scheme incorporates three fundamental source components: isotropic (ISO), double-couple (DC), and compensated linear vector dipole (CLVD), enabling comprehensive characterization of the source mechanism, including potential volumetric changes at the source.

Centroid depths were determined through a comprehensive 3D grid search algorithm. Green's functions were calculated using the frequency-wavenumber technique [Bouchon, 1981], incorporating a 1D velocity structure [Saetang, Duerrast, 2023] with frequencies up to 0.10 Hz. Density values for crustal layers were computed using:

$$\text{density (g/cm}^3\text{)} = 1.7 + 0.2 V_P \text{ (km/s)}.$$

The waveform processing methodology comprised multiple stages to optimize data quality. Initial preprocessing included instrumental response removal and baseline corrections to eliminate DC offsets and long-period trends. Both observed and synthetic waveforms underwent identical band-pass filtering within the 0.03—0.10 Hz frequency band. The lower frequency boundary (0.03 Hz) was established based on limitations imposed by long-period noise characteristics and instrument response constraints of the deployed seismometers. The upper frequency limit (0.10 Hz) was determined empirically, as higher frequencies exhibited poor waveform coherence across the network, likely due to the relatively large source-receiver distances.

The preprocessed seismic records were converted from counts to ground displacement in meters to facilitate quantitative analysis. We extracted 250-second time windows, beginning at the hypocentral time, which was

Table 1. Phase arrival times and location parameters for the November 9, 2023, M_w 4.1 earthquake

Station	Dist (km)	Azim (°)	Phase	HH:MM	t-obs	t_cal (s)	Δt (s)/res	Network
CMAI	73.2	48.9	PG	07:30	32.340	32.440	–0.10	TM
			SG		41.710	41.810	–0.10	
SMCM	75.8	162.5	PG	07:30	32.470	32.520	–0.05	TH
			SG		42.290	41.950	0.34	
CMTT	88.0	149.3	PG	07:30	34.530	34.640	–0.11	TM
			SG		45.170	45.550	–0.38	
MACM	98.6	52.6	PG	07:30	36.660	36.490	0.17	TH
			SG		48.790	48.700	0.09	
SUAB	108	80.2	PG	07:30	38.890	38.790	0.10	TM
			SG		52.760	52.610	0.15	

Note: Columns show station codes, epicentral distances (Dist), station azimuths (Azim), phase identifications (PG, SG), observation times (HH:MM, t_obs), theoretical arrival times (t_cal), arrival time residuals (Δt), and network affiliations (TM: Thai Meteorological Department; TH: Department of Mineral Resources).

sufficient to capture the complete wavefield for all analyzed events. The waveform data were resampled to 33 Hz to optimize computational efficiency while maintaining adequate temporal resolution. This systematic preprocessing sequence — incorporating instrument correction, band-pass filtering, unit conversion, time-window selection, and resampling — established a robust foundation for subsequent source parameter analysis.

The full waveform inversion minimized residuals between the observed and synthetic displacement waveforms using a least-squares approach. The procedure systematically explored trial source positions and origin times to determine optimal source parameters. Depth optimization utilized incremental steps defined by the Green's function parameterization, with each iteration evaluating the correlation between synthetic and observed waveforms to identify the best-fitting source depth.

The temporal grid search examined time shifts at 0.2-second intervals, spanning ±5.0 seconds relative to the HYPOCENTER-derived origin time. The optimal source location and timing parameters, determined through this comprehensive grid search, defined the centroid depth and time of the earthquake. These parameters were obtained by minimizing the misfit between observed and synthetic waveforms, providing fundamental constraints on the spatiotemporal characteristics of the seismic source.

The quality of waveform matching was quantified through a variance reduction criterion (var.red.), calculated as:

$$\text{var.red.} = 1 - \frac{E}{O},$$

$$E = \sum (O_i - S_i)^2 \ , \ O = \sum O_i^2 \ ,$$

where S and O represent synthetic and observed waveforms, respectively, summed over all available data. Higher variance reduction values indicate superior waveform fits.

The full waveform inversion methodology employed three-component seismic data to determine fundamental source parameters (strike, dip, and rake) following the iterative deconvolution approach of Kikuchi and Kanamori [1991]. The inversion utilized complete seismograms without segregating wave types, optimizing the fit between observed and synthetic waveforms through a systematic grid search over possible source positions and times. The correlation coefficient between observed and synthetic waveforms served as the primary criterion for determining the optimal centroid parameters.

Results and Discussion. Initial earthquake location analysis employing the SEISAN algorithm [Havskov, Ottemöller, 1999] determined the hypocenter at 19.498°N, 98.518°E with a focal depth of 10.4 km, yielding an RMS travel-time residual of 0.19 s. Phase arrival analysis, utilizing data from the local networks operated by the Thai Meteorological Department (TM) and the Department of Mineral Resources (TH), indicates systematic travel-time distributions across northern Thailand (see Table 1). Station CMAI (Δ=73.2 km, azimuth=48.9°) registered PG and SG phases at 32.340 s and 41.710 s, respectively, with arrival time residuals of –0.10 s for both phases. Station SMCM (Δ=75.8 km, azimuth=162.5°) recorded PG and SG phases at 32.470 s and 42.290 s, with residuals of –0.05 s and +0.34 s, respectively. Station CMTT (Δ=88.0 km, azimuth=149.3°) recorded PG and SG arrivals at 34.530 s and 45.170 s, with residuals of –0.11 s and –0.38 s, respectively. Stations MACM (Δ=98.6 km, azimuth=52.6°) and SUAB (Δ=108 km, azimuth=80.2°) exhibited systematic distance-dependent travel-time patterns, with MACM recording PG and SG phases at 36.660 s and 48.790 s (residuals: +0.17 s, +0.09 s), and SUAB phases at 38.890 s and 52.760 s (residuals: +0.10 s, +0.15 s).

Moment tensor inversion analysis, employing fixed epicentral coordinates, determined a centroid time of 2023-11-09 07:30:19.86 UTC (Δt=+0.78 s relative to origin time) and centroid depth of 2.5 km (Table 2). The focal mechanism solution comprises two nodal planes: plane 1 (strike=1°, dip=59°, rake=–148°) and plane 2 (strike=253°, dip=63°, rake=–35°), indicating a predominantly strike-slip faulting. The moment tensor decomposition yields a 75 % double-couple component with –1.2 %

CLVD contribution. The principal stress axes orientation indicates *P*-axis (azimuth=215°, plunge=43°) and *T*-axis (azimuth=308°, plunge=2°). The scalar seismic moment (*M*) of $1.424 \cdot 10^{15}$ N·m corresponds to M_w 4.1. The centroid location is determined at 19.498°N (±4.7 km) and 98.518°E (±1.6 km), with a solution variance reduction of 0.16.

Grid search analysis for source parameter optimization (Fig. 3) demonstrates maximum correlation coefficients at a depth of 2.5 km with a Δt of +0.78 s. The correlation matrix exhibits values exceeding 0.4 within the 2—4 km depth range, corresponding to double-couple components >70 %. The centroid depth determination, combined with correlation values and double-couple percentages, constrains the rupture nucleation within the upper crustal section along the NE-SW trending structure west of the Wiang Haeng fault system. The solution stability is demonstrated by a systematic decrease in correlation value from the optimal centroid parameters, with minimal depth-time trade-off patterns.

Analysis of spatiotemporal source parameters (Fig. 4) reveals the M_w 4.1 earthquake (2023-11-09, 19.498°N, 98.518°E) occurred at a distance of 17 km west of the N-S trending Wiang Haeng fault system (reference coordinates: 19.5°N, 98.68°E). The spatial distribu-

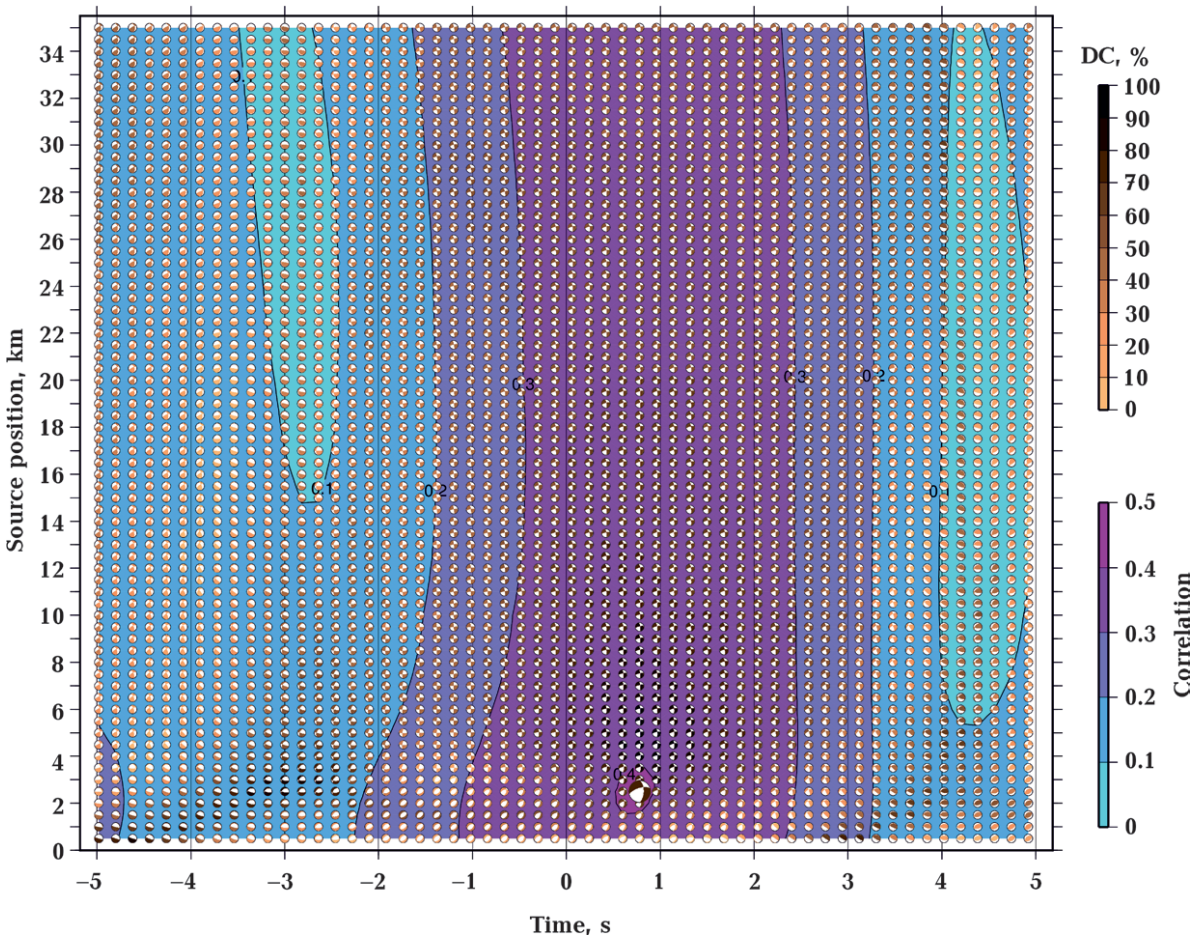

Fig. 3. Spatiotemporal grid search analysis for moment tensor optimization showing correlation coefficients as a function of centroid time and depth. The correlation matrix spans time shifts of –5 to +5 s relative to the initial origin time (horizontal axis) and source depths of 0—35 km (vertical axis). Correlation coefficients between observed and synthetic waveforms are represented by the cyan-blue-magenta color scale (right, 0.0—0.5), while the double–couple component percentages (0—100 % DC) are indicated by beach balls varying from light to dark gray. The optimal solution, marked by the largest beach ball, corresponds to a centroid depth of 2.5 km with a time shift of +0.78 s.

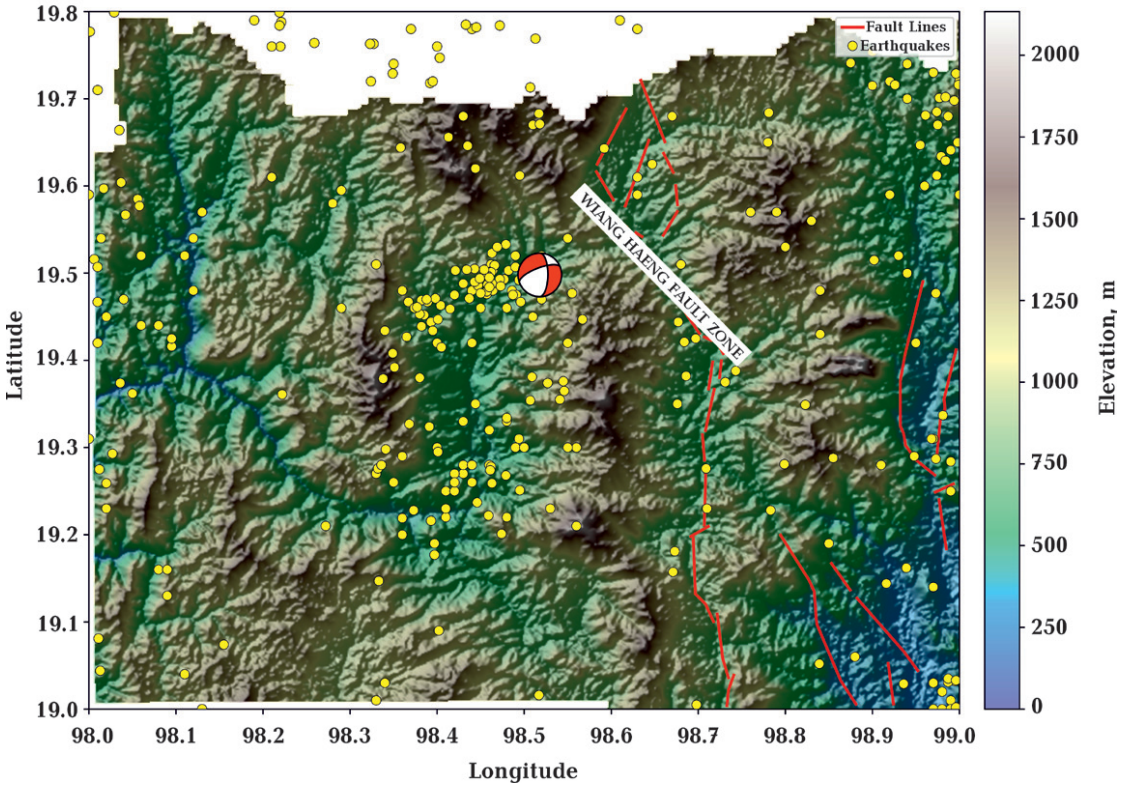

Fig. 4. Detailed topographic and seismotectonic map of the study area. The focal mechanism solution (beach ball diagram) for the November 9, 2023, M_w 4.1 earthquake (19.498°N, 98.518°E) is shown with red color. Yellow circles represent historical seismicity (2009-Nov 2024). Red lines denote mapped active fault traces. The digital elevation model (DEM) shows topographic variations from 0—2000 m, with color gradients from blue (low elevation) to brown (high elevation).

Table 2. Moment tensor inversion results with location uncertainty

Parameter	Value
Origin time (UTC)*	2023-11-09 07:30:19.08
Centroid time (UTC)	2023-11-09 07:30:19.86
Latitude (°N)	19.498 (±4.7 km)**
Longitude (°E)	98.518 (±1.6 km)**
Centroid depth (km)	2.5
Centroid time shift (s)	+0.78
Moment magnitude (M_w)	4.1
Scalar moment (N·m)	$1.424 \cdot 10^{15}$
Nodal plane 1 (Strike/Dip/Rake)	1°/59°/–148°
Nodal plane 2 (Strike/Dip/Rake)	253°/63°/–35°
P-axis (Azimuth/Plunge)	215°/43°
T-axis (Azimuth/Plunge)	308°/2°
Double-couple component (%)	75
CLVD component (%)	–1.2
Variance reduction	0.16

Note: *The origin time was determined using Seisan.
**Uncertainty values (±) are given in kilometers, as reported by Seisan.

tion of seismicity indicates a NE-SW alignment, oriented oblique to the mapped Wiang Haeng fault traces. The focal mechanism solution yields two potential fault planes. Based on the spatial correlation of seismicity distribution and structural orientations, nodal plane 2 (strike=253°, dip=63°, rake=–35°) represents the likely rupture plane. This interpretation is constrained by the geometric correspondence between the strike of nodal plane 2 and the NE-SW trending seismicity alignment in the source region, contrasting with the N-S orientation of the primary Wiang Haeng fault system.

The spatial distribution of seismicity and the focal mechanism solution indicate strain release along a NE-SW (253°) trending struc-

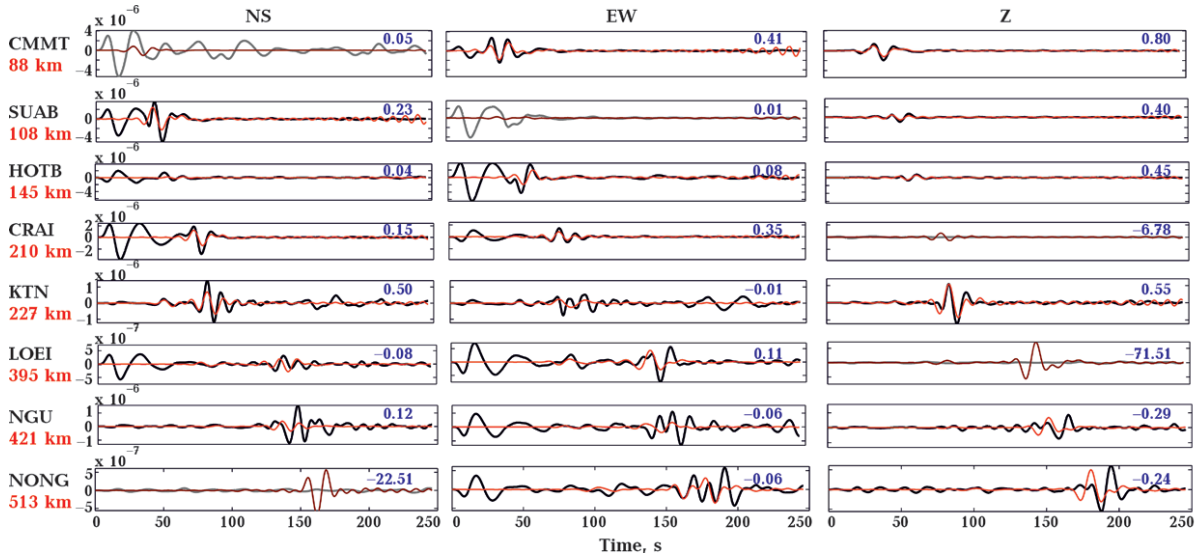

Fig. 5. Three-component waveform comparison between observed (black) and synthetic (red) seismograms at eight regional stations for the November 9, 2023, M_w 4.1 earthquake. Time series span 250 seconds starting from the origin time. Station codes and epicentral distances (km, red) are indicated at left. Variance reduction values (blue) are shown for each component. Gray traces indicate seismograms excluded from the inversion. All waveforms are band-pass filtered between 0.03—0.10 Hz. Amplitude scales are in meters.

ture, oriented oblique to the N-S trending Wiang Haeng fault system. This structural configuration suggests distributed deformation across multiple fault orientations within the upper crustal section, extending beyond the previously mapped fault traces (see Fig. 4).

Waveform analysis across the regional network (Fig. 5) demonstrates systematic variation in solution quality with epicentral distance. Variance reduction values at near-regional stations (CMMT: 88 km, SUAB: 108 km, HOTB: 145 km) range from 0.40 to 0.80 on vertical components. Stations at intermediate distances (CRAI: 210 km, KTN: 227 km) exhibit variance reductions between 0.35 and 0.55. The far-regional stations (LOEI: 395 km, NGU: 421 km, NONG: 513 km) show decreased variance reduction values, with significant negative coefficients in vertical components (–71.51 at LOEI, –0.29 at NGU). Observed and synthetic waveform comparisons within the 0.03—0.10 Hz frequency band indicate optimal fits for both *P* and *S* phases at stations within a 250 km epicentral distance.

Conclusions. Moment tensor inversion analysis of the M_w 4.1 earthquake (2023-11-09, 19.498°N, 98.518°E), located 17 km west of the Wiang Haeng fault system in northern Thailand, employing phase arrivals from local TM and TH network stations (Δ=73.2÷108 km), determined a centroid depth of 2.5 km with 75 % double-couple and –1.2 % CLVD components. The focal mechanism solution indicates predominantly strike-slip faulting, characterized by a strike of 253°, a dip of 63°, and a rake of –35°. Waveform analysis demonstrates variance reduction values ranging from 0.40 to 0.80 at near-regional stations (Δ<250 km). The spatial distribution of seismicity and the focal mechanism solution indicate strain release along a NE-SW (253°) trending structure, oriented oblique to the N-S trending Wiang Haeng fault system.

Acknowledgements. We gratefully acknowledge the Incorporated Research Institutions for Seismology for providing publicly accessible seismic data. We also extend our sincere appreciation to the Thai Meteorological Department and the Department of Mineral Resources of Thailand for permitting direct access to their non-public seismic network data. Their support was instrumental in the successful completion of this research.

Author Contributions. Kasemsak Saetang

conceived the study, developed the methodology, acquired and analyzed the data, interpreted the results, and drafted the initial manuscript. Wilaiwan Srisawat contributed to data acquisition. Both authors refined the methodology, reviewed, and edited the manuscript. They also conducted a critical review before submission. All authors have approved the submitted version.

Competing Interest Declaration. The authors declare no known financial or personal conflicts of interest that could have influenced the research presented in this manuscript.

References

Bouchon, M. (1981). A simple method to calculate Green's functions for elastic layered media. *Bulletin of the Seismological Society of America, 71*(4), 959—971. https://doi.org/10.1785/BSSA0710040959.

Earthquake catalog for Thailand and adjacent regions (in Thai). (2024). Thai Meteorological Department. Retrieved from https://earthquake.tmd.go.th/inside.html.

Geological map of Thailand. (2007). Department of Mineral Resources. Retrieved from https://shop.geospatial.com/publication/24M1N7DW45KJ4E257BFCC4DR57/Thailand-1-to-250000-Scale-Geological-Maps.

Havskov, J., & Ottemöller, L. (1999). SEISAN earthquake analysis software. *Seismological Research Letters, 70*(5), 532—534. https://doi.org/10.1785/gssrl.70.5.532.

Kikuchi, M., & Kanamori, H. (1991). Inversion of complex body waves: III. *Bulletin of the Seismological Society of America, 81*(6), 2335—2350. https://doi.org/10.1785/BSSA0810062335.

Lienert, B.R., Berg, E., & Frazer, L.N. (1986). HYPOCENTER: An earthquake location method using centered, scaled, and adaptively damped least squares. *Bulletin of the Seismological Society of America, 76*(3), 771—783. https://doi.org/10.1785/BSSA0760030771.

Lienert, B.R., & Havskov, J. (1995). A computer program for locating earthquakes both locally and globally. *Seismological Research Letters, 66*(5), 26—36. https://doi.org/10.1785/gssrl.66.5.26.

Morley, C.K., Charusiri, P., & Watkinson, I.M. (2011). Structural geology of Thailand during the Cenozoic. In M.F. Ridd, A.J. Barber, M.J. Crow (Eds.), *The geology of Thailand* (pp. 237—334). Geological Society of London. https://doi.org/10.1144/GOTH.11.

Noisagool, S., Boonchaisuk, S., Pornsopin, P., & Siripunvaraporn, W. (2014). Thailand's crustal properties from teleseismic receiver function studies. *Tectonophysics, 632*, 64—75. https://doi.org/10.1016/j.tecto.2014.06.014.

Saetang, K. (2017). Focal mechanisms of Mw 6.3 aftershocks from waveform inversions, Phayao Fault Zone, northern Thailand. *International Journal of Geophysics*. https://doi.org/10.1155/2017/9059825.

Saetang, K. (2022). Two-layer model of anisotropy beneath Myanmar and Thailand revealed by shear-wave splitting. *Annals of Geophysics, 65*(6), 1—13. https://doi.org/10.4401/ag-8769.

Saetang, K., & Duerrast, H. (2023). A minimum 1-D velocity model of northern Thailand. *Journal of Seismology, 27*, 493—504. https://doi.org/10.1007/s10950-023-10148-6.

Saetang, K., Srisawat, W., & Duerrast, H. (2018). Crustal structures, geothermal sources, and pathways beneath northern Thailand revealed by local earthquake tomography. *Chiang Mai Journal of Science, 45*(1), 565—575.

Simons, W.J.F., Socquet, A., Vigny, C., Ambrosius, B.A.C., Haji Abu, S., Promthong, C., Subarya, C., Sarsito, D.A., Matheussen, S., Morgan, P., & Spakman, W. (2007). A decade of GPS in Southeast Asia: Resolving Sundaland motion and boundaries. *Journal of Geophysical Research: Solid Earth, 112*, B06420. https://doi.org/10.1029/2005JB003868.

Sokos, E.N., & Zahradník, J. (2008). ISOLA: A Fortran code and a MATLAB GUI to perform multiple-point source inversion of seismic data. *Computers & Geosciences, 34*(8), 967—977. https://doi.org/10.1016/j.cageo.2007.07.005.

Seismic monitoring stations in Thailand (in Thai). (2024). Thai Meteorological Department. Retrieved from https://earthquake.tmd.go.th/stations.html.

Seismic station network (in Thai). (2024). Department of Mineral Resources. Retrieved from https://www.dmr.go.th/.

Tingay, M., Morley, C., King, R., Hillis, R., Coblentz, D., & Hall, R. (2010). Present-day stress field of Southeast Asia. *Tectonophysics, 482*(1—4), 92—104. https://doi.org/10.1016/j.tecto.2009.06.019.

Zahradník, J., & Plešinger, A. (2005). Long-period pulses in broadband records of near earthquakes. *Bulletin of the Seismological Society of America, 95*(5), 1928—1939. https://doi.org/10.1785/0120040210.

Фокальний механізм землетрусу 9 листопада 2023 р., M_w 4,1, у північній частині Таїланду, визначений інверсією повної форми хвилі

К. Саетанг[1], В. Шрісават[2], 2025

[1]Університет Накхонсітхаммарат Раджабхат, Накхонсітхаммарат, Таїланд
[2]Муніципальна школа Ваттапхо, Накхонсітхаммарат, Таїланд

Землетрус магнітудою 4,1 стався на півночі Таїланду (19,498° пн.ш., 98,518° сх.д.) 9 листопада 2023 р. (07:30:19,86 UTC) у межах сейсмічноактивного терейну Шан-Тай. Визначення параметрів джерела проводилося за допомогою повнохвильової інверсії з використанням трикомпонентних сейсмічних даних з десяти регіональних станцій на відстанях 73—108 км, що експлуатуються мережею сейсмічного моніторингу Департаменту метеорології Таїланду, мережею Департаменту мінеральних ресурсів Таїланду та Національною сейсмологічною мережею М'янми. У методології інверсії використовувався програмний пакет ISOLA, що реалізує ітеративну деконволюцію на основі шестиелементної структури тензора моментів. Методологія включала мінімальну одновимірну модель швидкості з корекціями станцій, каліброваними для північного Таїланду. Попередня обробка даних складалася з видалення інструментального відгуку, корекції базової лінії та смугової фільтрації. Функції Гріна були обчислені за допомогою інтегрування частоти та хвильового числа в смузі частот 0,03—0,10 Гц. Інверсія тензора моментів виявила переважно механізм скидозсуву з двома нодальними площинами: площина 1 (простягання=1°, падіння=59°, нахил=–148°) і площина 2 (простягання=253°, падіння=63°, нахил=–35°) з 75 % подвійної пари та –1,2 % CLVD-компонентів. Аналіз пошуку за сіткою систематично дослідив глибини джерел від 0 до 35 км і визначив оптимальну глибину центроїда (2,5 км) з максимальними коефіцієнтами кореляції, що перевищують 0,4 у діапазоні глибин 2—4 км. Аналіз хвильової форми демонструє зменшення дисперсії в діапазоні від 0,40 до 0,80 на станціях поблизу регіону (Δ<250 км), що свідчить про надійне визначення параметрів джерела. Фокальний механізм і розподіл сейсмічності вказують на вивільнення деформації вздовж структури, що простягається з північного заходу на південний схід, розташованої за 17 км на захід від системи розломів Віанг Хенг північно-південного простягання.

Ключові слова: фокальний механізм, повнохвильова інверсія, мінімальна 1D модель швидкості, північний Таїланд, сейсмотектоніка.